Towards a NEAMS-based high-fidelity model of the MARVEL reactor

INL/RPT-24-80887

Nuclear Energy Advanced Modeling and Simulation (NEAMS)

M2 Report

SEPTEMBER 2024

Stefano Terlizzi

Reactor Physics Methods and Analysis

Lise Charlot

Computational Frameworks

Idaho National Laboratory

Battelle Energy Alliance manages INL for the U.S. Department of Energy's Office of Nuclear Energy

INL/RPT-24-80887

Towards a NEAMS-based high-fidelity model of the MARVEL reactor

M2 Report

Stefano Terlizzi
Reactor Physics Methods and Analysis
Lise Charlot
Computational Frameworks

September 2024

Idaho National Laboratory
Nuclear Science and Technology
Idaho Falls, Idaho 83415

http://www.inl.gov

Prepared for the
U.S. Department of Energy
Office of Nuclear Energy
Under DOE Idaho Operations Office
Contract DE-AC07-05ID14517

Page intentionally left blank

SUMMARY

This report outlines the progress of Idaho National Laboratory in developing a high-fidelity multiphysics model of the Microreactor Applications Research Validation and Evaluation reactor, that is expected to start operation in 2027. The overarching objective of this activity funded by the Nuclear Energy Advanced Modeling and Simulation program, is the development of a high-fidelity multiphysics MARVEL model using NEAMS tools. This model is then be verified and validated against reference simulation and experimental data for MARVEL. This is a unique opportunity to conduct multiphysics analysis on a soon-to-be-deployed microreactor.

The multiphysics model presented in this report leverages three single-physics models coupled via the MOOSE's MultiApps and Transfer systems. The latter systems enable in-memory data transfer between MOOSE-based and MOOSE-wrapped applications. The first single-physics model, that functions as the driver application, leverages Griffin to model the neutron transport in the core through the discontinuous finite element (DFEM) discrete ordinates solver (SN). The second single-physics model uses BISON to compute the solid temperature in the reactor. Finally, the System Analysis Module (SAM) was used to model the flow of the sodium-potassium eutectic in the primary loop. A preliminary verification of the SAM model against the results in Ref. [1] was also performed, showing good agreement in terms of core mass flow rate as well as inlet and outlet temperatures. The full multiphysics model, that combines all the single physics models, was leveraged to conduct initial steady-state multiphysics simulations to compute power and temperature spatial distributions in the reactor core. While a reasonable agreement was shown for the thermal hydraulics calculations and multiphysics results, further verification is needed against reference results. An initial testing was performed for transient simulations as well.

Future work will focus on improving the fidelity of the multiphysics model. Additionally, we are planning to perform a comprehensive code-to-code comparisons vs. reference solutions provided by the MARVEL design team. Finally, further work will be performed to complete full-core transient simulations of a unprotected loss of flow scenario.

ACKNOWLEDGMENTS

The authors would like to acknowledge the contribution of Dr. Emily Shemon and Dr. Cody Permann for their feedback on the report, Dr. Yinbin Miao and Ishita Trivedi, for their help with the mesh generation, Dr. Namjae Choi for providing guidance on the use of optimization flags for the neutronics solver. We would also like thank the DOE Microreactor Program including Dr. John Jackson, Dr. Carlo Parisi, and Dr. Travis Lange for sharing MARVEL design specifications and physics insights on MARVEL which made this work possible.

Specific contributions:

1. Dr. Stefano Terlizzi - Conceptualization, Development of neutronics and thermal models; Formal analysis, Investigation, Writing, Review & editing, Visualization, Supervision.
2. Dr. Lise Charlot- Thermal Hydraulic model development and analysis, Writing, Review & editing, Visualization.

This research made use of the resources of the High Performance Computing Center at Idaho National Laboratory, which is supported by the Office of Nuclear Energy of the U.S. Department of Energy and the Nuclear Science User Facilities under Contract No. DE-AC07-05ID14517.

Page intentionally left blank

CONTENTS

FIGURES

TABLES

Page intentionally left blank

ACRONYMS

CRAB	Comprehensive Reactor Analysis Bundle
DOE	Department of Energy
INL	Idaho National Laboratory
MARVEL	Microreactor Applications Research Validation and Evaluation
MOOSE	Multiphysics Object-Oriented Simulation Environment
MRP	Micro-Reactor Program
NEAMS	Nuclear Energy Advanced Modeling and Simulation

Page intentionally left blank

Towards a NEAMS-based high-fidelity model of the MARVEL reactor

M2 Report

1. INTRODUCTION

The Microreactor Applications Research Validation and Evaluation design is a 85-kWth microreactor nuclear test-bed projected to start operations at Idaho National Laboratory in 2027 [4]. The Department of Energy-microreactor program recently reached 90% final design, a key step toward allowing the project to move forward with fabrication and construction. Once operational, MARVEL is envisioned to demonstrate several operating features of microreactors, including the investigation of diverse electrical and thermal applications and the evaluation of autonomous controls. A 3D rendition of the envisioned reactor is displayed in Fig. 1 [2]. The MARVEL design will use Uranium Zirconium Hydride (UZrH) for fuel and sodium-potassium eutectic (NaK) for coolant. Reactivity control is performed through four control drums employing boron carbide (B_4C). The reactor will utilize a power conversion system to generate up to approximately 20 kWe.

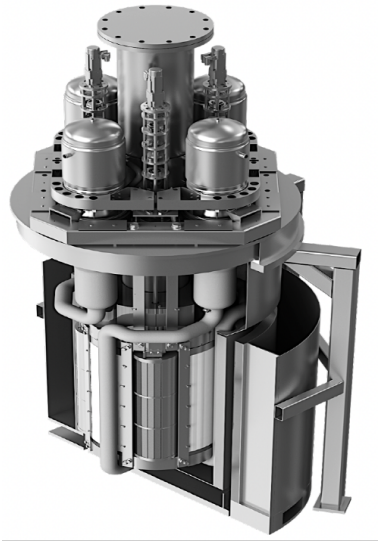

Figure 1. 3D rendition of the MARVEL reactor concept from [2].

This work reports the progresses made towards the development of a high-resolution and high-fidelity multiphysics model of MARVEL using NEAMS tools. The latter are a set of advanced modeling and simulation codes and capabilities funded by the DOE-NE to accelerate the deployment of advanced nuclear energy technologies through high-fidelity and high-resolution modeling and simulations. The model here described will lay the foundation for the next model's iteration where a comprehensive verification activities against the models produced by the MARVEL design teams in Fiscal Year 2025. The collaborative exercise between the NEAMS and the MARVEL design team is intended to be mutually beneficial, with data being provided to NEAMS and code capability being provided to the Micro-Reactor Program (MRP) to advance the deployment of microreactor technology.

The remainder of the report is structured as follows. Section 2. provides an overview of the MARVEL

reactor based on open literature, while the multiphysics model is detailed in Section 4.. Finally, results are reported in Section 5. and conclusions are drawn in Section 6..

2. DESCRIPTION OF THE MARVEL REACTOR CORE

The MARVEL core consists of 36 UZrH fuel elements. The reactor is cooled by NaK flowing in the gaps between the fuel pins due to natural circulation. The active core region is radially surrounded by a metallic beryllium internal reflector that follows the profile of the external pins' ring. The internal reflector is surrounded by a 316H stainless steel vessel and an external beryllium oxide (BeO) stationary reflector that houses the four control drums. Boron carbide (B_4C) is used as the absorbing material. Fig. 2 shows the radial view of the core mid-plane with ex-core components generated with the Monte Carlo N-Particles (MCNP) code by the MARVEL neutronic design team [3].

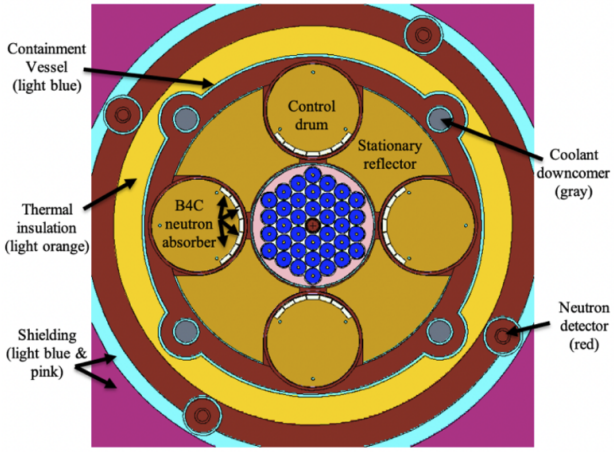

Figure 2. MARVEL core's mid-plane [3] with ex-core components.

The axial and radial view of the core without ex-core components is reported in Fig. 3. From the axial view, it is noticeable that the active fuel is axially surrounded by a top and bottom reflector. Zr filler rods are used to stuck the five fuel slugs and the graphite reflectors. The SS304 bottom and top end-caps engage with the respective support plate to keep the fuel elements in position.

3. CURRENT MODEL VS. MARVEL CORE

Several simplifications were made in the neutronic and solid heat transfer models, described in Sections 4.4.-5 respectively, to conduct the first multiphysics analysis with NEAMS-based tools. For instance, the *BeO* inner reflector geometry is approximated using a polygonal curve rather than a smooth curve following the curvature of the pins (as shown in the Serpent model in Fig. 6). Additionally, several ex-core structures are homogenized by volume in the Serpent, Griffin, and BISON model.

Due to the number of simplifications, the model described in this report is a *MARVEL-like reactor* that enables us to assess the ability of NEAMS-based tools to model small UZrH-fueled systems and MARVEL-like systems. In FY25, the model will be updated to align precisely with the MARVEL specifications. The

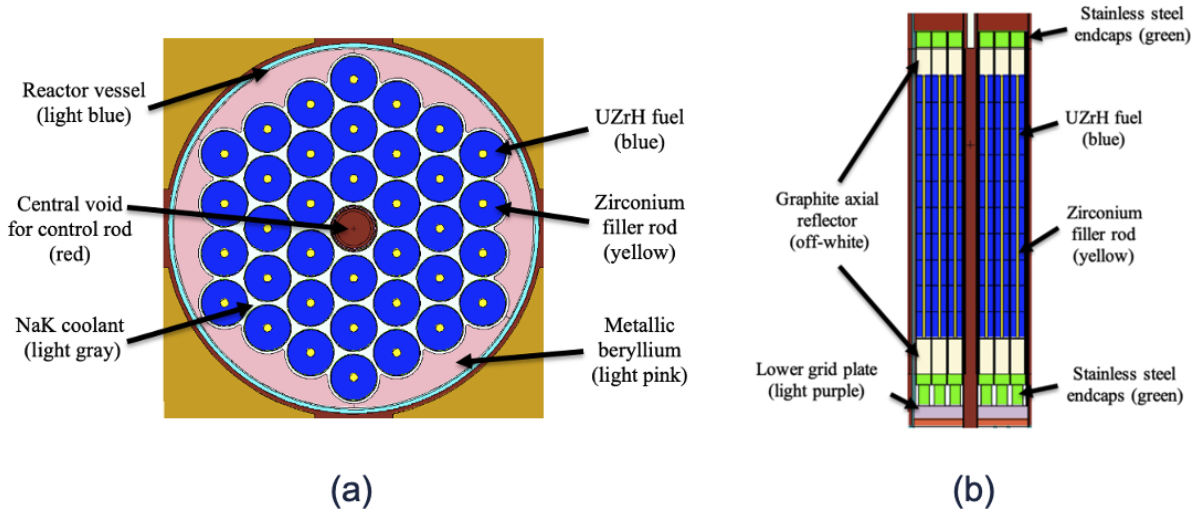

Figure 3. MARVEL core's (a) radial view with no ex-core components and (b) axial view [3].

updated FY25 model will also undergo a systematic verification of the neutronic model against reference MCNP and RELAP5-3D results.

4. MULTIPHYSICS MODEL

In this work, a reference multiphysics model for the MARVEL reactor was developed using Multiphysics Object-Oriented Simulation Environment (MOOSE)-based Comprehensive Reactor Analysis Bundle (CRAB) applications. The model integrates three single-physics simulations coupled through the MOOSE MultiApps system [5, 6]: (1) a Griffin neutronics model, which uses the discontinuous finite element method (DFEM) and discrete ordinates solver to compute neutron flux across the reactor, (2) a BISON model for simulating heat transfer in the solid components of the core, and (3) a SAM thermal-hydraulic model that simulates the NaK flow within the reactor using a single effective channel.

4.1. Coupling Scheme and Codes

The coupling scheme is shown in Fig. 4. Under steady-state conditions, the scheme is repeated at each Picard iteration and stops when the effective multiplication factor converges within an absolute tolerance of 10^{-8}. This tolerance was selected to ensure the convergence of the temperature field.

The **Neutronics** model, developed in Griffin, serves as the master application and is used to calculate the power density spatial distribution, denoted as P_d in Fig. 4. The power density is then transferred to the **Thermal Fluids** model that uses SAM to compute the NaK temperature as a function of height, denoted as T_c, the density spatial distribution, symbolized by ρ_c, and the heat transfer coefficient between the NaK and the fuel clad, h_c. The T_c and h_c are passed to the **Heat Transfer** model, developed in BISON, that computes the temperature of the solid, denoted by T_s. All the temperature and density fields are then used within Griffin to update the value of the few-groups cross sections. An overview of the transfers employed in the multiphysics coupling scheme is provided in Fig. 1, while the codes used for the single physics models and the preliminary operations of meshing and few-groups cross sections generation are reported in table 2. Sections 4.2.–4.6. report a detailed description of the preliminary operations and single physics models.

Table 1. Transferred quantities within the coupling scheme. The transfer numbers refer back to the labels used in Fig. 4.

Transfer Number	Transferred Quantities
a_1	$P_d; T_f; h_f$
a_2	$T_c; h_c; \rho_c$
b_1	P_d
b_2	T_s

Table 2. Codes used in solver blocks of Fig. 4.

Solver	Physics
Mesh	MOOSE
Cross Sections	Serpent
Neutronics	Griffin
Heat Transfer	BISON
Thermal Fluids	SAM

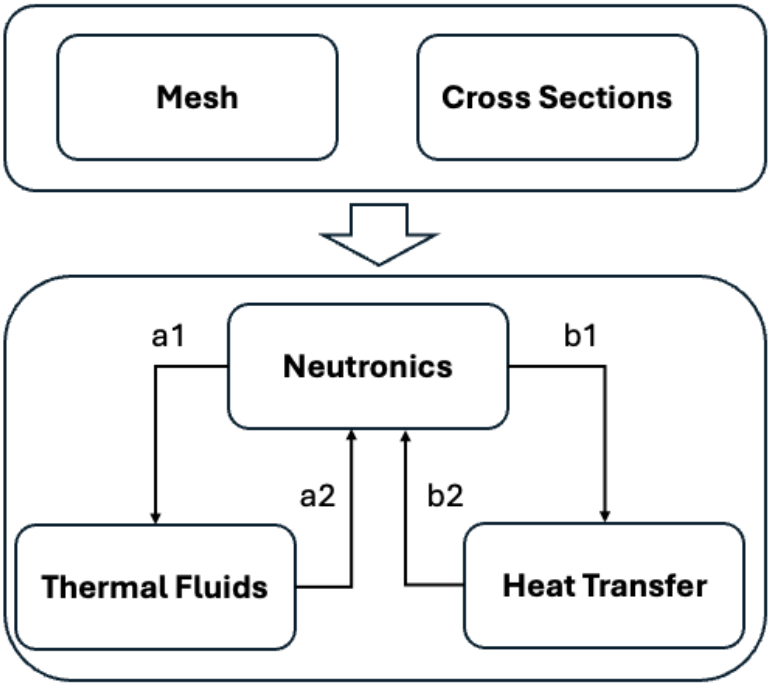

Figure 4. Multiphysics coupling scheme for steady-state calculations.

4.2. Meshing

The neutronic and thermal meshes were generated using the reactor module in MOOSE [7, 8]. This work constitutes one of the first cases in which the MOOSE reactor module was used to mesh irregular geometry (i.e., the geometry is irreducible to a Cartesian or hexagonal lattice). The neutronic mesh is shown in Figures 5, where a radial view of the core mid-plane and a 3D view of the core geometry are reported, respectively. The

recently implemented `ParsedCurveGenerator` and `XYDelaunay` triangulation features were used to mesh the quadrilobed external radial reflector. The latter two objects allow the modeler to mesh irregular geometries using general triangulation, provided the external curve bounding the subdomain is defined parametrically. The full 3D core mesh consists of 702,300 elements, with 46,820 elements per axial layer. A combination of triangular and rectangular elements is used to mesh the entire geometry.

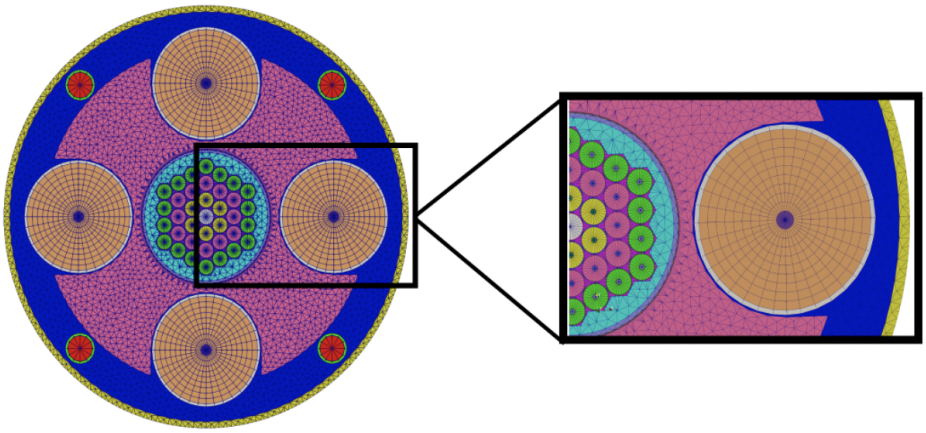

Figure 5. (a) View of mesh at the mid-plane and zoom-in for the inner reflector (in teal) showing the polygonal approximation.

4.3. Multigroup Macroscopic Cross Sections

Serpent (v.2) [9] with ENDF/B-VIII.0 continuous energy library was used to generate the few-groups macroscopic cross sections. The 13-group structure is tailored on the MARVEL spectrum and is based upon the Hansen-Rouch structure [10]. The energy bounds are shown in Fig. 3. The choice of the group structure was motivated by the similarities between MARVEL and SNAP8-ER in terms of material and dimensional specifications (*e.g.*, fuel type, reflector material, dimensions, etc...). The cross sections were generated using full-core isothermal eigenvalue calculations at intervals of 100 K, from a minimum temperature of 293 K to a maximum temperature of 1200 K. The dependence of the few-groups cross sections on temperature is captured by tabulating the macroscopic cross sections with respect to the local value of the temperature. The value of the cross sections for intermediate temperature values is reconstructed through linear interpolation.

Table 3. Energy group (upper) boundaries for the 13-group structure used in the Griffin model.

Group	Energy (MeV)	Group	Energy (MeV)
1	$2.00 \times 10^{+1}$	8	4.81×10^{-5}
2	8.21×10^{-1}	9	9.88×10^{-5}
3	1.83×10^{-1}	10	4.00×10^{-6}
4	4.90×10^{-2}	11	1.00×10^{-6}
5	2.10×10^{-2}	12	3.20×10^{-7}
6	1.90×10^{-3}	13	6.70×10^{-8}
7	4.54×10^{-4}		

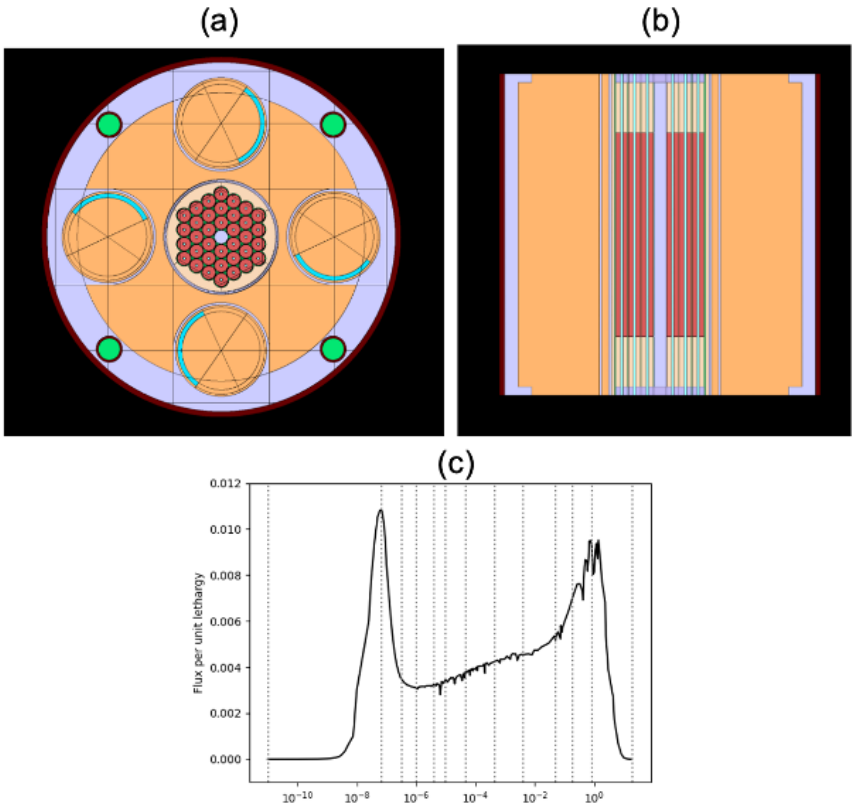

Figure 6. (a) Radial and (b) axial view of the MARVEL Serpent model. (c) Spectrum per unit lethargy for the full reactor (black line) and upper boundaries for energy group structure (dotted vertical line).

4.4. Neutronics Model

The neutron transport is simulated through the discrete ordinates multigroup model in Griffin [11]. Given a set of directions, $\{\hat{\Omega}_n\}_{n=0,\ldots,N-1}$, and weights, $\{w_n\}_{n=0,\ldots,N-1}$, where N is the total number of directions, the criticality form of the discrete ordinates (i.e., S_N), multigroup neutron transport equation reads as [12]:

$$\hat{\Omega}_n \cdot \nabla \psi_n^g(\vec{r}) + \Sigma_t^g(\vec{r})\psi_n^g(\vec{r}) = \mathcal{S}\phi^g(\vec{r}) + \frac{\chi^g(\vec{r})}{4\pi\, k}\mathcal{F}\phi(\vec{r}), \tag{1}$$

where:

- ψ_n^g is the angular flux in energy group g and along direction Ω_n,
- Σ_t^g denotes the total macroscopic cross section for group g,
- $\mathcal{S}$ is the scattering operator, defined as:

$$\mathcal{S}\phi^g(\vec{r}) = \sum_{g'=0}^{G-1}\sum_{n=0}^{N-1} w_n\, \Sigma_{s;n}^{g',g}\psi_n^{g'}(\vec{r}), \tag{2}$$

where the scalar flux is defined as:

$$\phi^g(\vec{r}) = \sum_{n=0}^{N-1} w_n\, \psi_n^g(\vec{r}). \tag{3}$$

- $\mathcal{F}$ is the fission operator:

$$\mathcal{F}\phi(\vec{r}) = \sum_{g'=0}^{G-1} \Sigma_f^{g'}(\vec{r})\phi^{g'}(\vec{r}). \tag{4}$$

- χ_g is the the fission spectrum.
- k is the effective multiplication factor.

The discontinuous finite element method (DFEM), is used for the spacial discretization. Additional, the Coarse-Mesh Finite Difference (CMFD) acceleration technique is here used to decrease the total number of transport sweeps, therefore minimizing the execution time of the simulation [13]. The CMFD acceleration equation is solved on a Cartesian mesh superimposed to the heterogeneous geometry. The Cartesian mesh is cubical with unit-cell pitch of 4 cm. The pitch was chosen based on a performance optimizations aimed at minimizing the number of Richardson iteration in criticality calculations.

4.5. Solid Heat Transfer Model

BISON was used to solve the heat conduction equation in the solid domains [14]:

$$\rho(\vec{r},t)c_p(\vec{r},t)\frac{\partial T(\vec{r},t)}{\partial t} = \nabla k(\vec{r},t)\ \nabla T(\vec{r},t) + \dot{q}(\vec{r},t), \tag{5}$$

where T represents the temperature, ρ is the density, c_p is the specific heat capacity, k is the thermal conductivity, and P_d is the heat source. Convective boundary conditions model the heat fluxes, $\vec{J}_q$, transferred to the sodium-potassium eutectic and at the periphery of the radial reflector:

$$\vec{J}_q(\vec{r},t)\cdot\vec{n} = h(\vec{r},t)\left(T(\vec{r},t) - T_{fluid}(\vec{r},t)\right), \tag{6}$$

where $\vec{n}$ is the outward normal unit vector to the surface, h is the heat transfer coefficient (HTC), and T_{fluid} is the fluid temperature. The environment temperature was set to 300 K with emissivity of 0.8 to account for radiative losses.

4.6. Thermal Fluids Model

SAM is used to model the primary loop of the reactor [15]. A diagram of the SAM model is shown in Fig. 7. The NaK coolant enters the rodded region through a lower plenum and is heated in the active core region. It rises due to buoyancy to the riser and enters the distribution plenum. It is slipped between the 4 heat exchangers. The heat exchanger are shell tubes and the secondary fluid is modeled as lead. Note that the secondary system in MARVEL will be using eutectic Gallium-Indium-Tin (eGa-In-Sn) as a coolant. The model will be updated in future work. The primary coolant is then redirected to the lower plenum through the downcomer pipes. There is no pump in the primary loop and the flow is driven by natural convection.

The core is modeled with a single channel coupled with a heat structure representative of the fuel rods. The lower and upper reflector regions are similar to the active core region but are not heated. The riser is modeled using two channels to account for the flow area change in the core barrel. The distribution plenum is a large 3D component that connects the risers with the 4 heat exchangers and the upper part of the riser below the argon cover. To model this complex part of the system in SAM, a `PBLiquidVolume` connects the riser with 4 small flow channels. This allows to specify the NaK level and the system pressure. Each

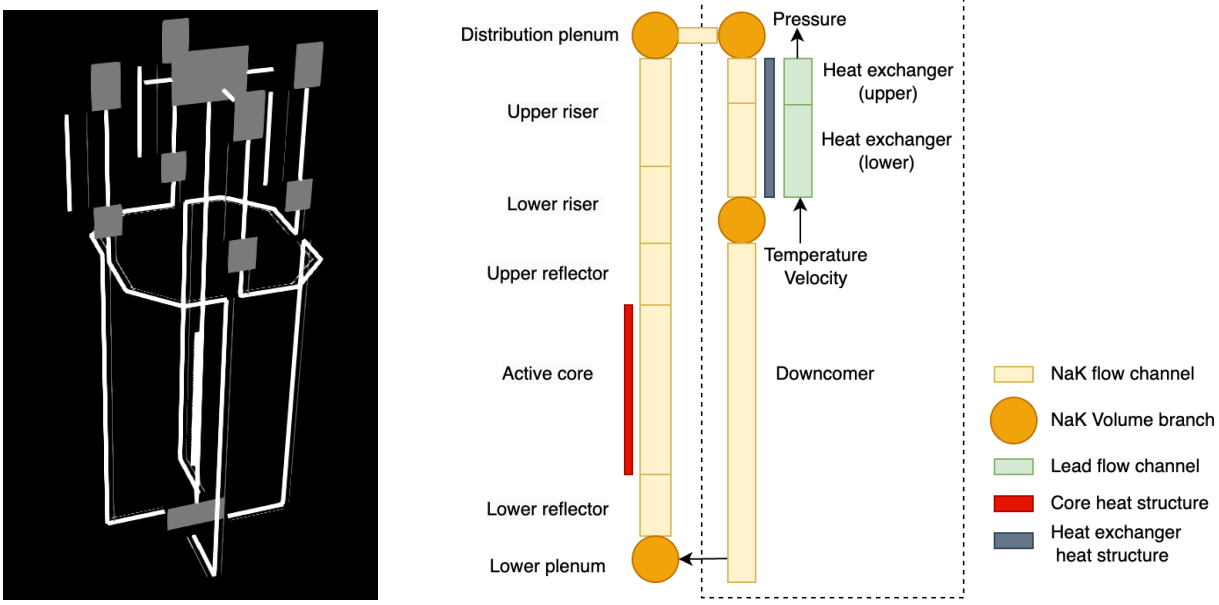

(a) 3D rendering of the SAM model (b) Diagram of the SAM model

Figure 7. SAM model of the primary loop

flow channel is connected to a volume branch that is then connected to the heat exchanger of the loop. The volume of the volume branches, channels and liquid volume in the distribution plenum have been calculated to preserve the total volume of the distribution plenum. The heat exchangers are shell-tube heat exchangers with counter-current flow. They are modeled using the `PBHeatExchanger` component. The secondary side is using lead as the coolant. The secondary loop is not included in this model. Instead, inlet velocity and temperature are prescribed at the secondary inlet of the heat exchanger and a back pressure is applied at the outlet. The values of these boundary condition has been taken for normal operation from [1]. The downcomer is modeled with a series of flow channels to represent the 3D layout of the loop. Each flow channel is coupled to a heat structure to model the thermal inertia of the associated pipe. This model assumes there is no heat loss, which is a difference with the RELAP-5 model described in [1]. All the geometric input parameters required by the SAM model (flow areas, heated perimeters, component length, etc.) have been calculated using the MARVEL drawing and CAD models provided by the MRP. The friction factor in the core is calculated using the Cheng-Todreas correlation [16] and the heat transfer coefficient is evaluated with the updated Calamai/Kazimi-Carelli correlation[17]. The form loss coefficient for each junction has been set to 0.2 to match the expected mass flow rate in the loop.

5. RESULTS

This section presents the results from the initial verification of the neutronics and thermal-hydraulics calculations, along with the multiphysics steady-state calculations. Preliminary considerations on transient simulations are also included. Lastly, a section detailing the optimization of the neutronic solver's performance is provided.

5.1. First Neutronics Verification

The verification of the Griffin neutronic model against reference Serpent (v.2) results was performed for three problems of increasing difficulty, starting from a unit cell problem to a full 3D core. A view of the geometries for the three problems, denoted by P1–P3 is shown in Fig. 8. A more detailed explanation follows:

1. **P1** is a 2D pseudo unit cell, in which a cladded UZrH pin radial cross-section (in red) is surrounded by NaK coolant (in green). The geometry of the pseudo unit cell is reported in the first row of Fig. 8. Reflective radial boundary conditions are imposed to the 2D problem.

2. **P2** is 2D core problem, formed by a radial cross section of the 3D MARVEL core at the mid-plane. Vacuum boundary conditions are imposed radially. The geometry of the 2D core is represented in the second row of Fig. 8.

3. **P3**. The 3D full-core problem is the P2 problem extruded in the vertical direction and completed with axial reflector. The radial and axial view of the Serpent geometry together with the 3D core mesh is displayed in the last row of Fig. 8.

The comparison between reference continuous energy Monte Carlo and Griffin results are performed in terms of both effective multiplication factor and power distribution (when applicable). The power distribution's error is characterized through the maximum error, denoted by e_{max}, and the L2 norm of the error, denoted by e_{mean}, while the multiplication factor is compared in terms of relative difference. The e_{max} and e_{mean} are both computed pin-wise. The results of these comparisons are reported in Table 4 for the three problems. It is noticeable that the agreement is within 352 pcm for the 3D core. The error in pin-wise power distribution is within 2.1% in all cases. Additional fine-tuning will be necessary to further reduce this error.

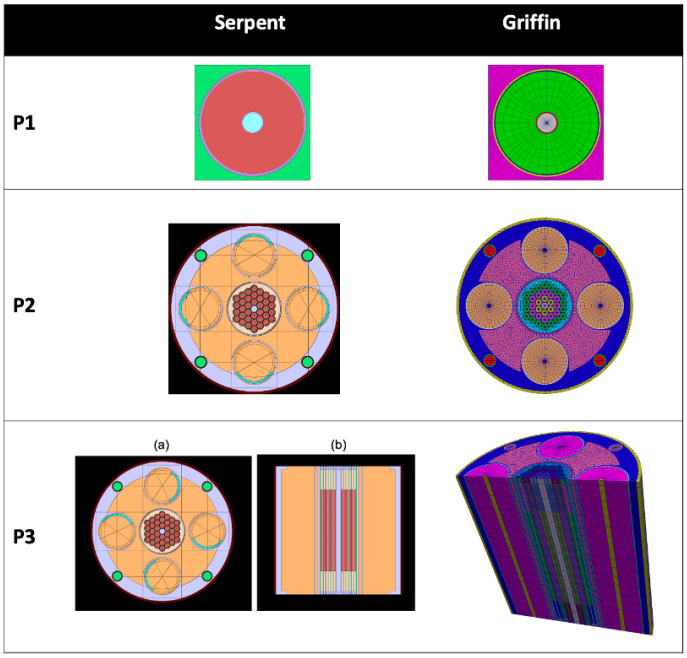

Figure 8. Verification problems for the Griffin neutronics model.

Additional verification was performed to ensure the correctness of the feedback mechanisms for the full 3D core. Table 5 reports the Doppler fuel feedback and the isothermal temperature feedback. The Doppler

Table 4. Comparison of Griffin results vs. reference Monte Carlo calculations. Value for on standard deviation are reported in parenthesis. For δ_k/k, the standard deviation is reported in per cent miles (pcms).

Problem	$\delta k/k$	e_{max}	e_{mean}
P1	3 (2)	N/A	N/A
P2	210 (2)	1.7 (0.13%)	1.1 (0.11%)
P3	352 (3)	2.1 (0.31%)	1.4 (0.24%)

feedback was calculated by varying homogeneously the temperature of the fuel from 293 K to 1200 K, while the isothermal thermal feedback was computed by performing the same operation on the whole reactor. By inspecting Table 5, we can notice that a good agreement within 0.2 pcm/K is achieved in both cases. Future work will be focused on a more detailed comparison between Serpent reference and Griffin results, including group-wise reaction rates (*e.g.* fission and capture) and selected values of the control drums insertion angle.

Table 5. Doppler and isothermal coefficients in pcm/K

Feedback	Serpent	Griffin
Fuel	-5.11 (0.20)	-4.90
Isothermal	-3.45 (0.25)	-3.30

5.2. First Thermal Hydraulics Verification

An initial verification of the SAM thermal hydraulics model was performed to ensure its consistency with the RELAP5-3D calculations in Ref. [1]. The comparison for the inlet, outlet temperature, and mass flow rate is reported in Table 6, while the NaK temperature distribution is reported in the Fig. 9. The latter shows the coolant temperature increasing from 752 K to 818 K in the core representative channel before being collected in the upper plenum and being subsequently redistributed in the four downcomers. To obtain the temperature reported in the figure, a flat power profile normalized to the total power of 85 kWth was used. From Table 6, it is noticeable that the inlet and outlet temperatures differ of 14 K with respect to the reference values, while the mass flow rate difference is around 4.5%. This is justifiable based on differences between the SAM and RELAP5-3D model, such as the distributed pressure loss formula, and the use of a single representative channel in lieu of a ring-wise radial discretization of the NaK flow. Consistently with the neutronics model, additional fine-tuning and adjustments will be performed on the model to improve fidelity. This will be the object of additional work in fiscal year 2025.

Table 6. Comparisons of key T/H quantities. The RELAP5-3D values are reported from Ref. [2].

	SAM	RELAP5-3D
Core mass flow rate [kg/s]	1.46	1.53
Core inlet temperature [K]	752	738
Core outlet temperature [K]	818	805

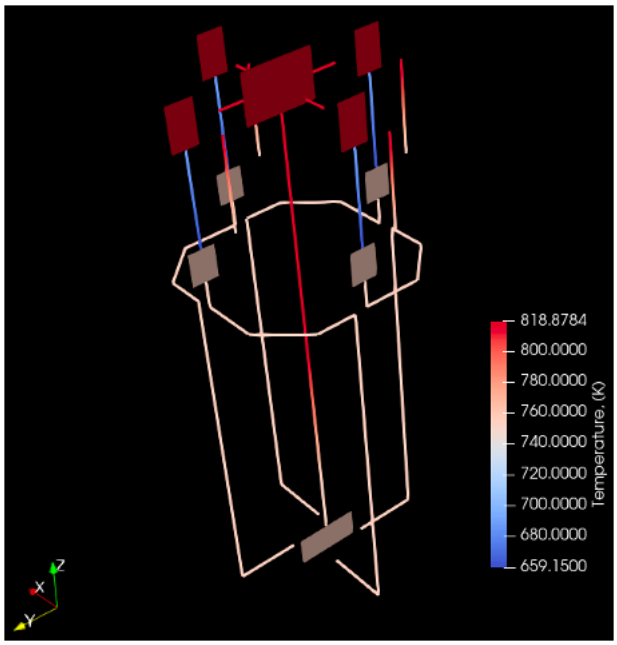

Figure 9. Temperature distribution in the primary loop

5.3. Steady State Multiphysics Calculation

The multiphysics steady-state solution was run by utilizing 480 processors in INL's Sawtooth high-performance computing cluster. The simulation wall-clock time totalled 46 minutes and used the coupling scheme explained in Section 4.1.. For this multiphysics steady state calculation, seven Picard iterations were performed to reach converged temperature and power distribution. The number of Picard iteration is chosen to converge with respect to the effective multiplication factor within a relative tolerance in 10^{-8}. The relative tolerance on the effective multiplication factor was chosen to converge within 10^{-6} in relativer error for the maximum fuel temperature. In order to minimize the memory usage, the mesh pre-splitting capability for both the heat transfer and neutronics single-physics models was used. The latter enabled the simulation to be run without exceeding memory limits on Sawtooth nodes.

Fig. 10 illustrates the steady-state values of the power density distribution and coolant temperature. It is noticeable, that the coolant temperature reaches 824 K at the core outlet. Notably, the temperature difference between the inlet and outlet is 66 K, a value close to 61 K that is reported in Ref. [2]. The axial power density distribution is sinusoidal due to the constant fuel enrichment. A more interesting trend is exhibited by the power density spatial distribution in the mid-plane, as shown in Fig.11.a. In fact, it is evident that power peaks in the outer fuel elements' ring that faces the radial reflector. A sub-pin spatial gradient develops because the inner part of the fuel element faces the coolant, while the outer part faces the radial reflectors, thus resulting in a high number of neutrons being scattered back into the fuel to produce additional power. A similar trend is observed for the thermal flux, shown in Fig.11.b. This highlights the potential of using a high-resolution method, such as DFEM-SN in Griffin, which can capture local gradients that would be difficult or impossible to capture with legacy nodal codes or Monte Carlo methods. Further studies will be necessary to confirm these gradients after improving the thermal-hydraulic feedback, as the geometry of the reflector causes higher heat transfer in the outer regions compared to the inner side, thus mitigating the gradients seen in Fig. 11.

Finally, the solid temperatures were computed using BISON. Fig.12.a–c show the temperatures for the fuel, inner reflector, and outer reflector, respectively. The maximum fuel temperature is 823 K, with the

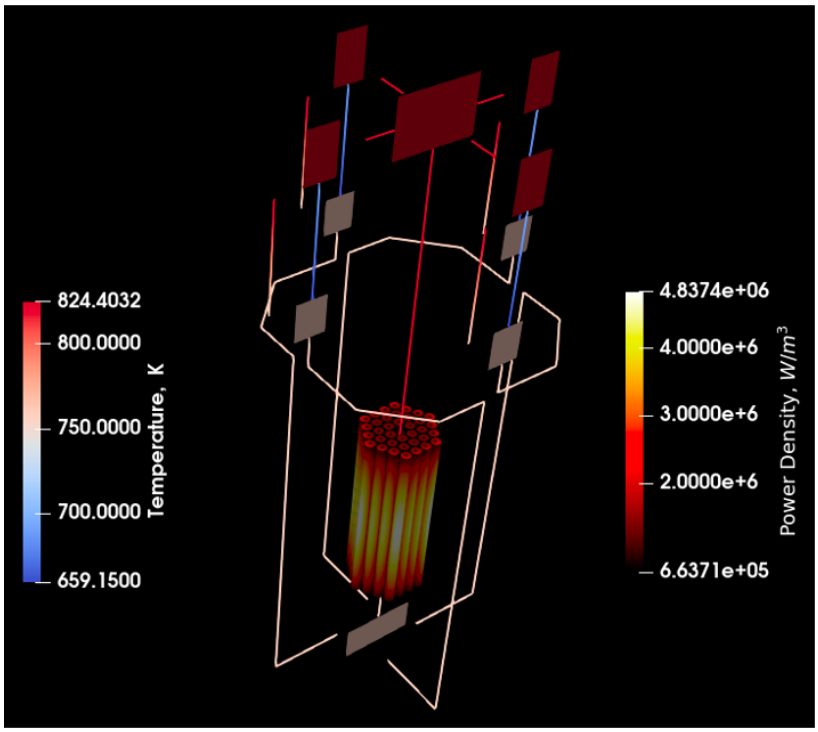

Figure 10. Power Density distribution in the fuel and coolant temperature

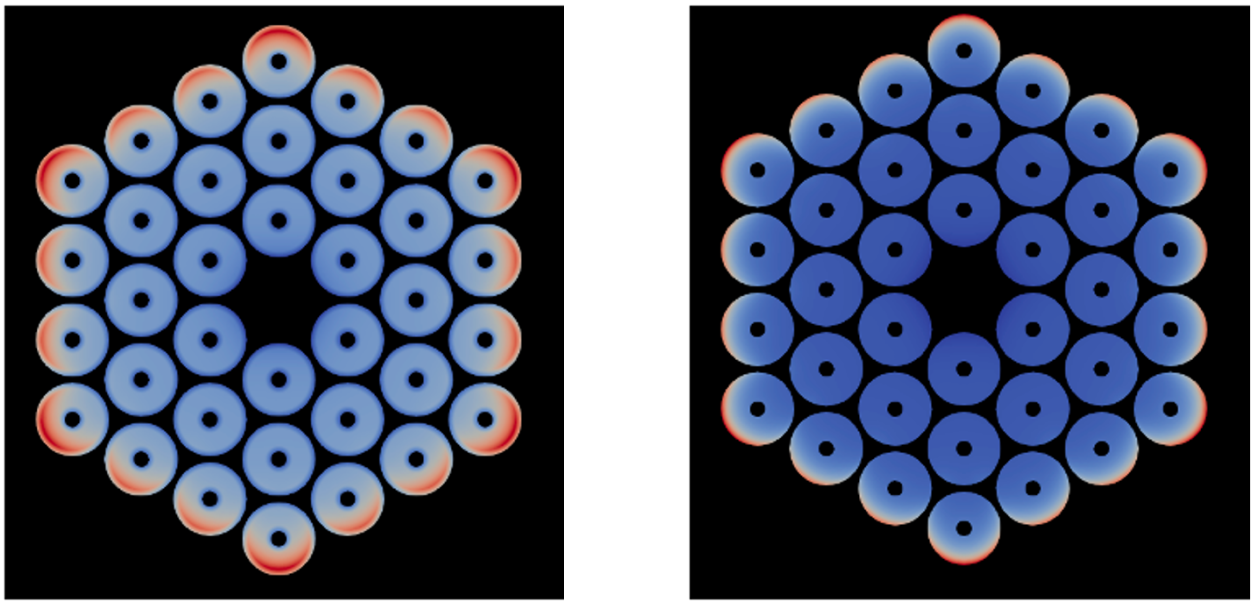

(a) (b)

Figure 11. (a) Power density and (b) thermal flux radial distributions in the fuel mid-plane.

temperature of the inner reflector being close to it (i.e., maximum temperature of the inner reflector is 816 K). The current model predicts a temperature drop of about 100 K from the inner to the outer reflector due to the presence of an argon-filled gap between the two radial reflector. In future research, additional analyses will be conducted to improve the modeling of gap conductance, as these results differ from those in Ref. [1], where

the temperature decrease is reported to be negligible.

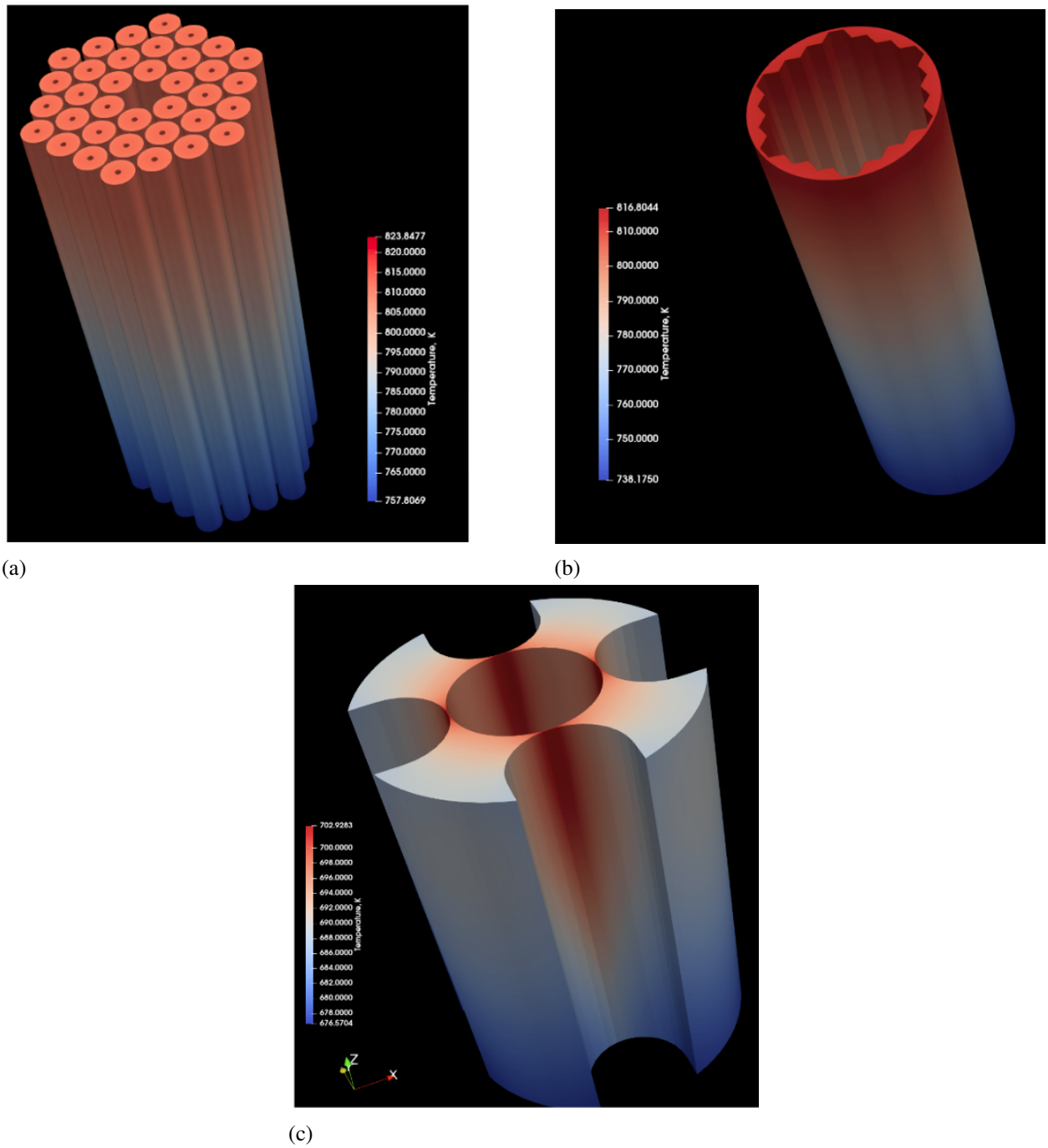

(a) (b)

(c)

Figure 12. Temperature spatial distribution for (a) fuel, (b) inner reflector, (c) outer reflector.

5.4. Neutronics Performance Optimization

Due to the computational expense of full-core multiphysics calculations, efforts were directed towards optimizing BlueCRAB's performance through collaboration with the Griffin development team. Through

these optimizations, the execution time for a full-core steady-state neutronics calculation was reduced from about 7.5 minutes on 480 processors to 2 minutes on the same number of processors.

- `using_average_xs` and `update_averaged_xs_on`.. These two flags included in the `TransportSystem` block enable the users to avoid the costly on-the-fly cross-section evaluation at each quadrature point by leveraging element-averaged cross-sections that have been already stored in the sweeper. Additionally,this option allows users to control the frequency of cross-section update instead of calling it on every residual evaluation. In this work, the cross sections were updated only at the beginning of each fixed point iteration due to the update of the temperature field in the core. To exemplify their use, the `TransportSystem` block is displayed in Fig. 13 As pointed out in Ref. [18], "the residual evaluation also benefits from this option by utilizing pre-assembled elemental matrices (such as mass matrix) in the sweeper instead of doing numerical quadrature evaluation. CMFD acceleration also benefits from this option by using pre-stored element averaged cross sections in coarse-mesh homogenization instead of evaluating quadrature point-wise cross sections on-the-fly with the MOOSE assembly system, which substantially reduces the CMFD projection time." It is to be noticed that these flags are currently not extended in case of displacement or mesh adaptivity. The extension of the capabilities to capture the thermomechanical feedback and to enable the use of mesh adaptivity will be pursued in Fiscal Year 2025.

```
[TransportSystems]
  equation_type = eigenvalue
  particle = neutron
  G = 13
  VacuumBoundary = 'external top bottom'
  [sn]
    scheme = DFEM-SN
    n_delay_groups = 6
    family = MONOMIAL
    order = FIRST
    AQtype = Gauss-Chebyshev
    NPolar =  2
    NAzmthl = 6
    NA =      2
    using_averaged_xs = true
    update_averaged_xs_on = 'INITIAL MULTIAPP_FIXED_POINT_END'
  []
```

Figure 13. Transport System Block in Griffin.

- **`fixed_point_outer`**. The parameter is used in the `Executioner` block to enforce the fixed point logic based upon the convergence of the effective multiplication factor. Through `fixed_point_outer`, the coupling between neutronics and the thermal hydraulic feedback is performed every "N" Richardson iterations. This overruns the standard coupling logics employed in the DFEM-Sn, where the feedback on neutronics is computed at each Richardson iteration. The use of the `fixed_point_outer` flag leads to to a 2-folds speed up in the multiphysics steady-state calculations. This is because the duration of a single thermal hydraulic calculation is much longer than a single Richardson iteration. The `Executioner` block for this work is reported in Fig. 14.

5.5. Initial Transient Considerations and Ongoing Work

Ongoing work is focused on performing a full-core transient calculation using the DFEM-SN solver and verifying it against RELAP5-3D simulations conducted by the MARVEL design team [1]. Specifically, an Unprotected Loss of Flow (ULOF) scenario is under investigation, which involves a complete blockage of the four downcomers at the start of the transient, without any control mechanism insertion. In this scenario, the reactor will rely solely on negative temperature feedback for shutdown, with heat being dissipated primarily through radial conduction and radiation.

```
[Executioner]
  type = SweepUpdate
  verbose = false
  debug_richardson = false
  # Richardson solver parameters
  richardson_value = eigenvalue
  richardson_abs_tol = 1e-5
  richardson_rel_tol = 1e-5
  richardson_max_its = 2
  inner_solve_type = GMRes
  max_inner_its = 2
  truncate_scat_order = 0
  # CMFD acceleration
  cmfd_acceleration = true
  coarse_element_id = coarse_element_id
  diffusion_eigen_solver_type = newton
  prolongation_type = multiplicative
  uniform_group_collapsing = 5
  # Fixed point iteration
  fixed_point_solve_outer = true
  fixed_point_algorithm = picard
  custom_pp = eigenvalue
  custom_rel_tol = 1e-50
  custom_abs_tol = 1e-6
  force_fixed_point_solve = true
  fixed_point_max_its = 10
[]
```

Figure 14. Executioner Block in Griffin.

An initial simulation, testing the new checkpoint restart capability for eigenvalue problem was performed to enable a streamlined restart of the neutronic model from an eigenvalue calculation to a transient [19]. The restart worked correctly by demonstrating the ability to withhold a null transient for a Griffin DFEM-SN transient simulation without thermal feedback. Additional work will be necessary to test the capability for full-core neutronics with feedbacks.

6. CONCLUSIONS AND FUTURE WORK

This report outlines the progress of Idaho National Laboratory in developing a high-fidelity model of the Microreactor Applications Research Validation and Evaluation reactor. The model was developed under the Nuclear Energy Advanced Modeling and Simulation microreactor application driver at Idaho National Laboratory and was enabled through collaboration with the DOE Microreactor Program. The overarching objective of this activity is the development of a high-fidelity multiphysics MARVEL model using NEAMS tools, and to verify and validate NEAMS tools against MARVEL reference simulation and experimental data, respectively.

In this report, we describe the development of a first multiphysics model of the MARVEL reactor based on NEAMS-based tools. This first reference plant model leverages Griffin to simulate the neutron transport in the core, BISON to handle the solid heat transfer, and the System Analysis Module (SAM) to model the flow of the sodium-potassium eutectic in the primary loop. Several features recently implemented in MOOSE-based tools, such as features to mesh irregular geometry, flag for the neutronic solver's optimization, and the checkpoint restart, were here tested to enable this work scope. A first comparison between the results computed from the NEAMS-based multiphysics model vs. open literature for the MARVEL reactor was also performed to build confidence in the modeling and simulation procedure. While a reasonable agreement was shown for the thermal hydraulics calculations and multiphysics results, further verification is needed against reference results.

Future work will focus on improving the fidelity of the models. For instance, we are planning to substitute the single-channel SAM model with a more complex SAM-Pronghorn coupled model, in which the sub-

channel capability is deployed to obtain radial temperature resolution in the coolant. This model will be developed in synergy with the NEAMS thermal hydraulics team. More importantly, we are planning to perform a comprehensive and systematic code-to-code comparisons against reference solutions provided by the MARVEL design team. In particular, the full-core Griffin neutronics model will be benchmarked against MCNP reference results provided by the design team, while the SAM T/H model will be verified against reference RELAP5-3D results for selected accident scenarios. Finally, additional work will be performed to complete full-core transient simulations of a unprotected loss of flow scenario.

7. REFERENCES

[1] C. Parisi and Y. Arafat, "Marvel thermal-hydraulics: Normal and accidental conditions," in *ANS Transactions*, 2022. American Nuclear Society Winter Meeting.

[2] D. Gerstner, Y. Arafat, J. Andrus, and J. Parry, "Safety design strategy for the microreactor applications research validation and evaluation (marvel) project," in *ANS Transactions*, vol. 127, pp. 1078–1081, 11 2022.

[3] T. Lange, A. Wagner, C. Parisi, and Y. Arafat, "Marvel core design and neutronic characteristics," in *ANS Transactions*, 2022. American Nuclear Society Winter Meeting.

[4] "Marvel Microreactor Reaches Final Design Step," 2023.

[5] G. Giudicelli, A. Lindsay, L. Harbour, C. Icenhour, M. Li, J. E. Hansel, P. German, P. Behne, O. Marin, R. H. Stogner, J. M. Miller, D. Schwen, Y. Wang, L. Munday, S. Schunert, B. W. Spencer, D. Yushu, A. Recuero, Z. M. Prince, M. Nezdyur, T. Hu, Y. Miao, Y. S. Jung, C. Matthews, A. Novak, B. Langley, T. Truster, N. Nobre, B. Alger, D. Andrš, F. Kong, R. Carlsen, A. E. Slaughter, J. W. Peterson, D. Gaston, and C. Permann, "3.0 - MOOSE: Enabling massively parallel multiphysics simulations," *SoftwareX*, vol. 26, p. 101690, 2024.

[6] D. R. Gaston, C. J. Permann, J. W. Peterson, A. E. Slaughter, D. Andrš, Y. Wang, M. P. Short, D. M. Perez, M. R. Tonks, J. Ortensi, L. Zou, and R. C. Martineau, "Physics-based multiscale coupling for full core nuclear reactor simulation," *Annals of Nuclear Energy*, vol. 84, pp. 45–54, 2015.

[7] E. Shemon and et al., "Moose reactor module: An open-source capability for meshing nuclear reactor geometries," *Nuclear Science and Engineering*, pp. 1–25, 2023.

[8] A. D. Lindsay and et al., "2.0 - MOOSE: Enabling massively parallel multiphysics simulation," *SoftwareX*, vol. 20, p. 101202, 2022.

[9] J. Leppänen and et al, "The serpent monte carlo code: Status, development and applications in 2013," *Annals of Nuclear Energy*, vol. 82, pp. 142–150, 2015.

[10] I. N. Aguirre, S. Garcia, B. Lindley, S. Terlizzi, A. Abou Jaoude, and D. Kotlyar, "Verification of the serpent-griffin workflow using the snap 8 experimental reactor," in *International Conference on Mathematics and Computational Methods Applied to Nuclear Science and Engineering (M&C2023)*, 8 2023.

[11] Y. Wang, Z. M. Prince, H. Park, O. W. Calvin, N. Choi, Y. S. Jung, S. Schunert, S. Kumar, J. T. Hanophy, V. M. Labouré, C. Lee, J. Ortensi, L. H. Harbour, and J. R. Harter, "Griffin: A moose-based reactor physics application for multiphysics simulation of advanced nuclear reactors," *Annals of Nuclear Energy*, vol. 211, p. 110917, 2025.

[12] W. F. Miller and E. E. Lewis, *Computational Methods of Neutron Transport*. American Nuclear Society, 1993.

[13] Z. M. Prince, J. T. Hanophy, V. M. Labouré, Y. Wang, L. H. Harbour, and N. Choi, "Neutron transport methods for multiphysics heterogeneous reactor core simulation in griffin," *Annals of Nuclear Energy*, 2023. Submitted for publication.

[14] R. L. Williamson and et al., "Bison: A flexible code for advanced simulation of the performance of multiple nuclear fuel forms," *Nuclear Technology*, vol. 207, no. 7, pp. 954–980, 2021.

[15] L. Zou, G. Hu, D. O'Grady, and R. Hu, "Code validation of sam using natural-circulation experimental data from the compact integral effects test (ciet) facility," *Nuclear Engineering and Design*, vol. 377, p. 111144, 2021.

[16] S. Cheng and N. Todreas, "Hydrodynamic models and correlations for bare and wire-wrapped hexagonal rod bundles-bundle friction factors, subchannel friction factors and mixing parameters," *Nuclear Engineering and Design*, vol. 92, pp. 227–251, 1986.

[17] G. Calamai, R. Coffield, L. Jossens, *et al.*, "Steady State Thermal and Hydraulic Characteristics of the FFTF Fuel Assemblies," Tech. Rep. ARD-FRT-1582, Westinghouse Electric Corporation, 1974.

[18] C. Lee, Y. S. Jung, S. Kumar, N. Choi, J. T. Hanophy, and Y. Wang, "Improved fast reactor capability of griffin in fy23," Research Report INL/RPT-23-74897-Rev000, Idaho National Laboratory, June 2023.

[19] "Skip initialization when restarting an eigenvalue calculation #27621." https://github.com/idaholab/moose/issues/27621. Accessed: 2024-09-24.